

ornl

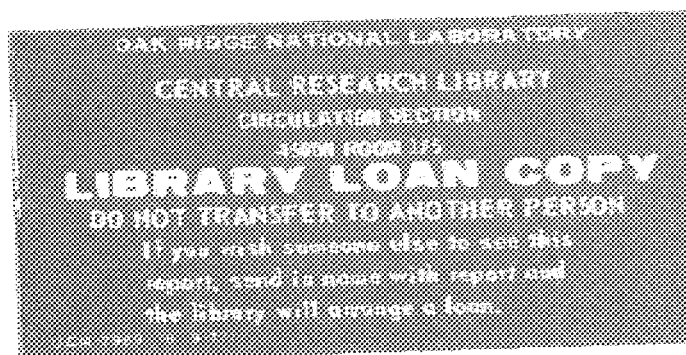
ORNL/TM-10763
(CESAR-88/07)

**OAK RIDGE
NATIONAL
LABORATORY**

MARTIN MARIETTA

Treatment of Systematic Errors in the Processing of Wide Angle Sonar Sensor Data for Robotic Navigation

M. Beckerman
E. M. Oblow



OPERATED BY
MARTIN MARIETTA ENERGY SYSTEMS, INC.
FOR THE UNITED STATES
DEPARTMENT OF ENERGY

Printed in the United States of America. Available from
National Technical Information Service
U.S. Department of Commerce
5285 Port Royal Road, Springfield, Virginia 22161
NTIS price codes—Printed Copy: A03; Microfiche A01

This report was prepared as an account of work sponsored by an agency of the United States Government. Neither the United States Government nor any agency thereof, nor any of their employees, makes any warranty, express or implied, or assumes any legal liability or responsibility for the accuracy, completeness, or usefulness of any information, apparatus, product, or process disclosed, or represents that its use would not infringe privately owned rights. Reference herein to any specific commercial product, process, or service by trade name, trademark, manufacturer, or otherwise, does not necessarily constitute or imply its endorsement, recommendation, or favoring by the United States Government or any agency thereof. The views and opinions of authors expressed herein do not necessarily state or reflect those of the United States Government or any agency thereof.

ORNL/TM-10763
CESAR-88/07

Engineering Physics and Mathematics Division

TREATMENT OF SYSTEMATIC ERRORS IN THE PROCESSING OF WIDE ANGLE SONAR
SENSOR DATA FOR ROBOTIC NAVIGATION

M. Beckerman and E. M. Oblow

Research sponsored by the Office of Basic Energy Sciences
and the Office of Technology Support Programs,
U.S. Department of Energy

Date Published: April 1988

Prepared by the
Oak Ridge National Laboratory
Oak Ridge, Tennessee 37831
operated by
Martin Marietta Energy Systems, Inc.
for the
U.S. DEPARTMENT OF ENERGY
under Contract No. DE-AC05-84OR2140



3 4456 0275172 4

TABLE OF CONTENTS

	Page
ABSTRACT	vii
1. INTRODUCTION	1
1.1 Experimental Testbed	1
1.2 Systematic Errors	1
1.3 Objectives and Methodology	2
2. INFORMATION PROCESSING	5
2.1 Possible Interpretations of an Isolated Return ...	5
2.2 Multiple Returns and Patterns of Conflict	6
2.3 Labels and Their Logic	6
2.4 Pattern Analysis	8
3. MAPS AND ANALYSES	11
3.1 Laboratory Environment and Robot Navigation	11
3.2 Instantaneous Scan Maps and Strings	12
3.3 Cumulative Navigation Maps	13
3.4 Consistent-Labeling	15
3.5 Discussion of Results	16
4. DISCUSSION OF SOME ALTERNATIVE APPROACHES	19
5. SUMMARY AND CONCLUDING REMARKS	21
Acknowledgements	21
References	23

INDEX TERMS

Information Processing

Mobile Robots

Sonar Range Sensing

Navigation

Map-Building

Feature-Extraction

Pattern Analysis

Consistent-Labelling

Uncertainty

ABSTRACT

A methodology has been developed for the treatment of systematic errors which arise in the processing of sparse sensor data. We present a detailed application of this methodology to the construction from wide-angle sonar sensor data of navigation maps for use in autonomous robotic navigation. In the methodology we introduce a four-valued labelling scheme and a simple logic for label combination. The four labels, conflict, occupied, empty and unknown, are used to mark the cells of the navigation maps; the logic allows for the rapid updating of these maps as new information is acquired. The systematic errors are treated by relabelling conflicting pixel assignments. Most of the new labels are obtained from analyses of the characteristic patterns of conflict which arise during the information processing. The remaining labels are determined by imposing an elementary consistent-labelling condition.

1. INTRODUCTION

In this work we describe a methodology for the treatment of systematic errors which arise in the processing of sparse sensor data. We introduce the various components of the methodology while presenting a detailed application to the processing of sonar range information for use in navigation by the HERMIES-IIB mobile robot of the Center for Engineering Systems Advanced Research (CESAR) at the Oak Ridge National Laboratory (ORNL). The function of the methodology in this application is to enable the robot to build a reliable internal spatial representation of the world, i.e., a navigation map, for which there is otherwise no prior information.

1.1 Experimental Testbed

HERMIES-IIB is one of a series of research robots designed for autonomous navigation in unknown and possibly hazardous terrain. The robot is discussed in depth by Burks, de Saussure, Weisbin, Jones and Hamel.[2] In brief, it is equipped with vision sensors, an on-board 16-node NCUBE hypercube parallel computer, and an on-board AT host computer. The HERMIES-IIB robot is also equipped with 24 ultrasonic range sensors. The sensors are grouped into a 6-phased-arrays of 4 units each. The units contained Polaroid industrial-grade transducers, and produced a chirp at a frequency of 50 KHz.

The sonar units function as both transmitter and receiver. In the sensing process the time-of-flight for the returned signal is measured. Given the velocity of sound, the range to the scattering source is then determined. Intensity information is not recorded; instead, the earliest return signal is processed. Thus, the distance to the nearest object lying either wholly or partially within the beam cone is determined, and the region lying inside the beam cone at shorter distances than that of the scattering source is established as being unoccupied.

In the experiments, range data were taken in 15-degree steps over the full 360 degree field. The beam width and angular acceptance of the sonar units are broad. In the phased configuration, the main beam lobe is approximately 18 degrees wide (valley-to-valley). The selection of a 15-degree angular stepsize is based on the observation that, because of the broad beam width and angular acceptance, data collected in smaller steps are highly redundant. The stepsize chosen allows for a useful overlap between adjacent data points as well as providing an efficient probe of the test space.

1.2 Systematic Errors

The sonar range sensors, as used, give rise to a variety of systematic errors (see, for example,[10]). By systematic errors we

mean those errors which result from incorrect and inconsistent interpretations of the data during processing. The sonar systematic errors depend upon the number, sizes, orientations and surface characteristics of the constituents of the world to which the robot is probing, as well as on the properties of the robot's sensors. By definition of the testbed, we do not have sufficient information about the constituents of the robot's world to be able to correct for the systematic errors during the initial processing.

Instead, we observe that there are several possible interpretations of the data from a given isolated scan. When combining data from different scans erroneous initial interpretations will give rise to recognizable patterns of conflict. Whenever this happens we can replace the erroneous interpretations with those which are consistent with the updated information. Not all systematic errors can be so treated, and such a methodology is best suited to the case where the data are sparse, and where the patterns of conflict are simple and the corrections unambiguous.

1.3 Objectives and Methodology

There are distinct conflict identification and resolution stages in our methodology. In the identification stage four labels are introduced to delineate occupied, empty, unknown and conflict cells of the robot's map. A simple logic is then used to combine data from different scans. In the resolution stage physical arguments are incorporated into pattern analyses and consistent labelling conditions to modify initial interpretations of the data. In this nonlocal approach we make explicit use of the correlated nature of the data, and we ensure that the methodology is robust.

The extent to which we are successful in identifying and resolving the resulting conflicts and uncertainties is determined by examining the two-dimensional navigation maps constructed from the sonar data. These maps should have accurately and clearly delineated open spaces and obstacles. Another objective is to ensure that the methodology allows for the extraction of progressively higher-level features which may be integrated with the commensurate vision data.

The importance of computation maps as key building blocks in the infrastructure of the low and intermediate level information processing in the nervous system has been documented in studies by Knudsen, du Lac and Easterly[18], Takahashi and Konishi[26] and Sullivan and Konishi[25]. For example, computational maps of interaural delay, interaural intensity difference and space all contribute to the spatial analysis of sound. Although our maps are not computational maps in the nervous system, they do serve an analogous physiological function. These maps are, of course, software constructs designed for a machine and its sensors. At the present level of sensor integration the maps are the robot's

internal representation of the world. It is therefore important to examine the roles played by higher-level inferencing in the constructing of such maps from sparse and incomplete data.

The tools used in our methodology are presented in Section 2. Their introduction is preceded by a discussion of the lowest level of information processing and the existence therein of an underlying world-view. Several types of spatial maps are created. We describe these maps and examine the overall performance of the methodology in Section 3. Other researchers in the field have developed local strategies for building navigation maps. We compare our approach to some of the alternative methods in Section 4 and summarize our work in Section 5.

2. INFORMATION PROCESSING

2.1 Possible Interpretations of an Isolated Return

The principal systematic errors are those related to the broad beam width and large angular acceptance of the sensors. Displayed in Fig. 1 are schematic representations of some of the possible interpretations of the scan return from a single scan angle. The arcs drawn in the figure denote the angular width of the beams, which was taken as 18 degrees. These arcs are shown superimposed upon a rectangular grid defining the bins (pixels) into which the information will be stored. The situation depicted in (a) corresponds to interpreting the scattering source as lying along the centerline (beam axis) at the distance given by the rangefinder. A single pixel, not lying along the beam axis, is viewed as being occupied by the scattering source in (b) and in (c); a pair of pixels are occupied in (d), and all pixels intercepted by the arc are interpreted as the scattering source in (e).

ORNL-DWG 88M-7341

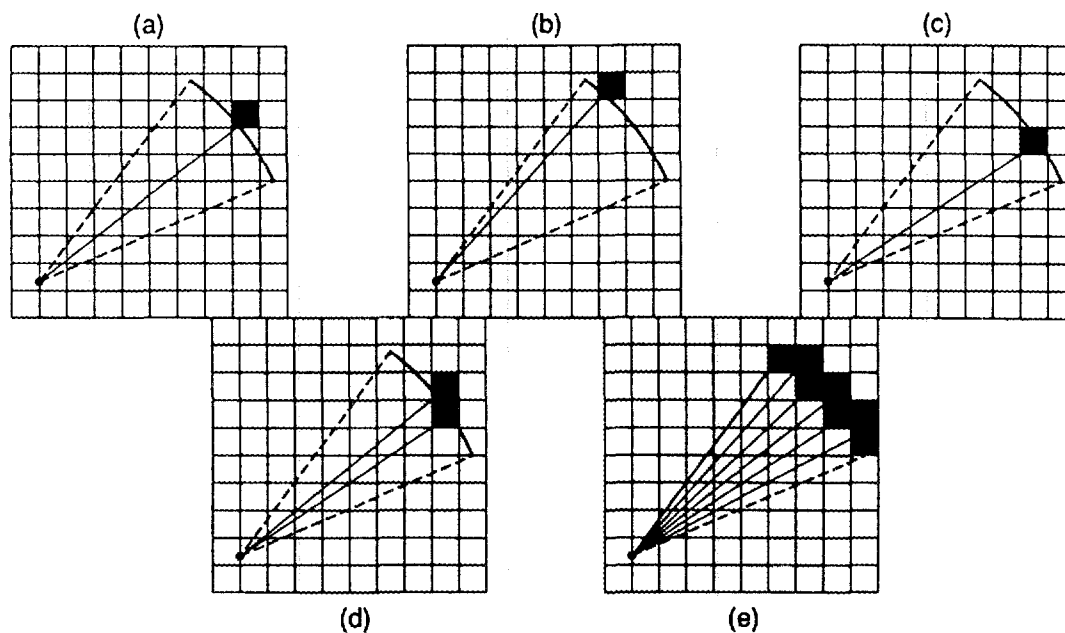


Fig. 1. Plot of five possible interpretations of an isolated return from a single scan. The arcs are not drawn to scale in this and the following figures.

Processing our sparse data we initially adopt interpretation (e), in which all possible occupied pixels are taken as such, to be the one best representing the scattering source. Underlying this choice is a world-view, specifically, that the robot's universe consists of extended objects (relative to the geometric size of a pixel). This world-view may be contrasted to, say, one for a world containing only well-separated point-objects. In such a point-object world, possibilities (a) to (c) would be more appropriate.

The implementation for a single isolated return consists of labelling those pixels lying along the arc as occupied and scoring all pixels located inside the region bounded by the endpoint rays and the arc as empty. All other pixels, for which there was no information from the robot's sensors, were marked as unknown. In the processing of the data all pixels were initially considered as unknown. To identify the pixels located along the beam arcs, additional returns, of identical range, were generated (by the software) at intermediate angles. A stepsize of 3 degrees was chosen as being adequate to cover the region of interest. The unoccupied region was then swept out by finding all pixels intercepted by the rays drawn at each intermediate angle from the occupied domain to the origin.

2.2 Multiple Returns and Patterns of Conflict

In Fig. 2 we represent data from two scan returns covering a common region of interest. In (a) and (b) we depict the returns from a pair of adjacent scan angles from a single observation point. In (c) and (d) the robot is scanning overlapping regions of space from two different viewing points. In each of the four examples, there is some conflict in the results of applying interpretation (e) (of Fig. 1) to the scan pairs. The methodology at this point consists of identifying the conflict generated among the pixel labels, and then resolving this conflict to achieve a consistent interpretation of the data.

2.3 Labels and Their Logic

To process the information from two (or more) scans, we perform pixel by pixel multiplication using the rule of combination

$$L_{ij}^A \cap L_{ij}^B = L_{ij}^C \quad .$$

In the above L_{ij} denotes the label for the ij^{th} pixel, and the superscripts A and B identify the pair of measurements leading to

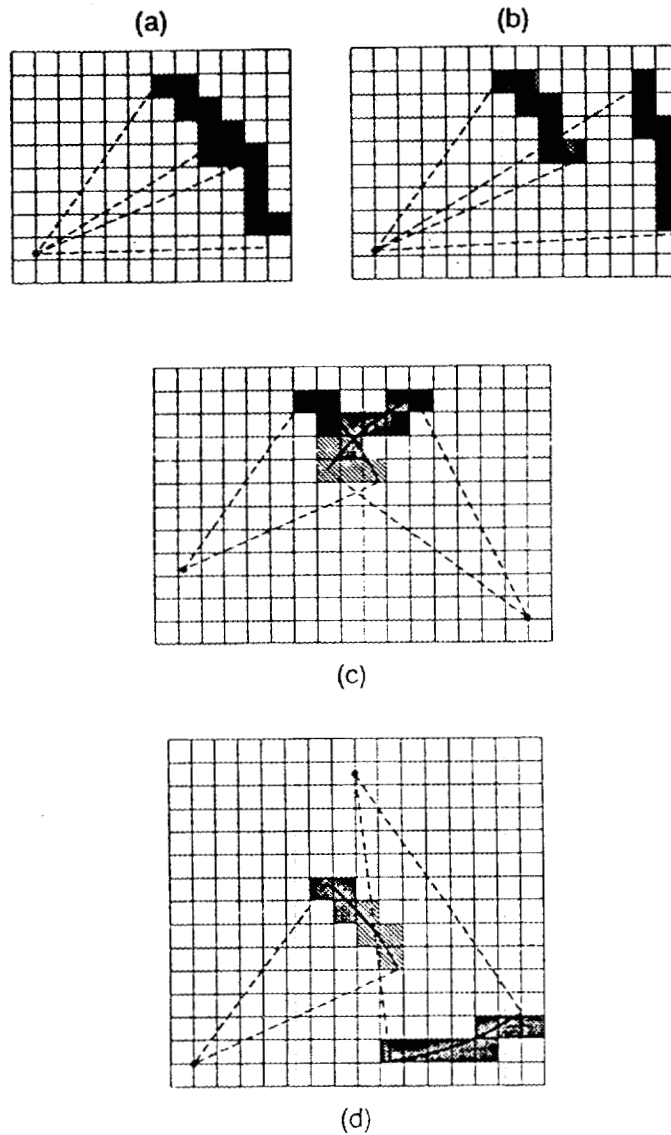


Fig. 2. Plot of representative pixel patterns. Heavily shaded cells denote occupied pixels. Cross-hatched cells have conflicting label assignments.

the new result C. The conflict label differs from the occupied and empty labels in that two returns are needed for its assignment. In set terminology, we may use the conflict element to represent the simultaneous intersection of occupied and empty elements. If we define the unknown element as the union of occupied and empty, we can use the intersection operator as our rule of label combination, as indicated in the above expression. The following figure (Fig. 3) gives the results so derived:

ORNL DWG 88M-7342A

		L^B				
		*	C	U	O	E
L^A	C	C	C	C	C	
	U	C	U	O	E	
	O	C	O	O	C	
	E	C	E	C	E	

Fig. 3. Logic for label combination.

with $C = O \cap E$ and $U = O \cup E$.

An essential feature of this possibilistic, labelling scheme is its binary character, that is, one and only one label per pixel. This labelling representation allows for the pattern analyses discussed in the next section. It may be noted that two of the labels, U and C, are in a sense, placeholders for the physical labels, O and E.

The pixel by pixel multiplication was coded using the label representation:

$$C = 0, U = 1, O = 2, \text{ and } E = 3.$$

The sixteen possible binary products were then evaluated by executing the statement

$$\text{if } L^A = L^B, \text{ then } L^C = L^A; \text{ else } L^C = L^A \times L^B \text{ mod } 6.$$

The first (if) part of this statement (written above in an obvious, nontechnical notation) handles the four diagonal entries in the table, while the twelve off-diagonal elements were handled by the second (else) part, and $L = C, U, O, \text{ or } E$. Returning to Fig. 2, we find that conflict pixel labels are assigned in the overlap region where the cells are marked empty in one case and occupied in the other.

2.4 Pattern Analysis

In Fig. 4 we present the analyzed and corrected interpretations of the patterns initially given in Fig. 2. We see in these diagrams that all uncertain pixel assignments have been resolved with the replacement of conflict with empty labels. The physical reason for this replacement is that a real sonar beam cannot pass through a real object in its path.

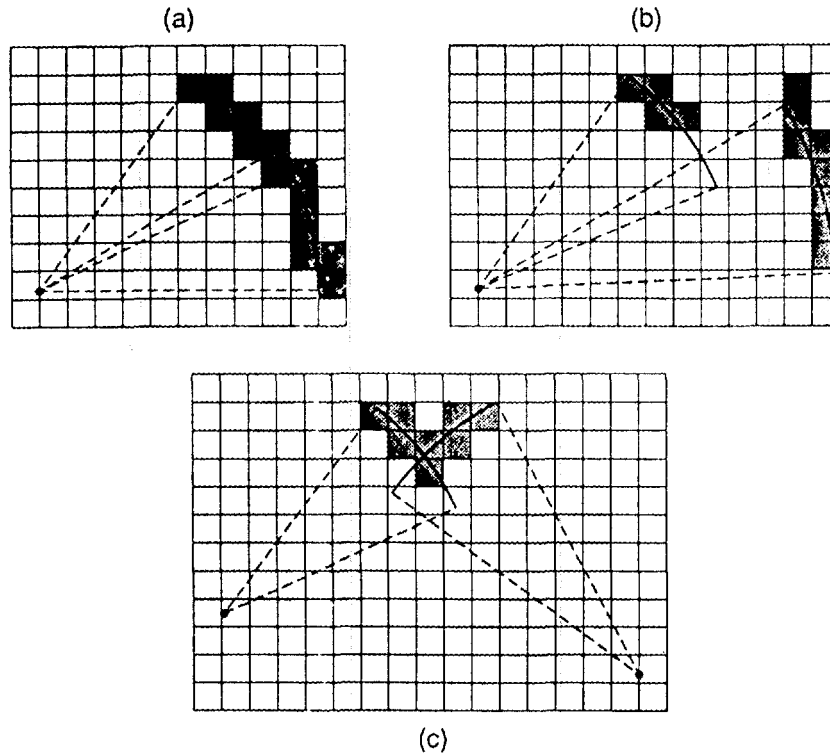


Fig. 4. Corrected plot of representative pixel patterns. Shown in this figure are pixel patterns (a) to (c) of Fig. 2 after the pattern analysis.

For instance, the systematic error flagged by the conflict label in (a) arises as a result of a slight disparity between the (curved) locus of possible occupied cells and the actual surface of the object. Specifically, the arcs tend to identify pixels which are progressively too close to the beam origin as the surface normal increasingly departs from orthogonality to the beam direction. The correct interpretation is to take the longer of the two possible returns at each viewing angle as being correct, since those returns should lie closer to the actual surface.

In (b) we have an example where the two arcs have rather different ranges. If the ranges are similar, we have situation (a), and we assume that there is a single extended scattering source and apply the correction just discussed. If the ranges are not similar, then

we may assume that there is more than one scattering source. If the cells in question were occupied, then the longer of the two returns would not have been received. Thus, the only consistent interpretation is that the pixels with conflicting labels are empty. The effect of this correction upon the nearby object is similar to that of a shrinking (as opposed to a dilation) operation in vision information processing.

The situation shown in (c) arises because the initial processing using the maximal set (Fig. 1 [e]) tends to exaggerate the spatial extent of surfaces. We correct for this as additional data are collected by relabelling as empty those pixels which are flagged by the ensuing conflicts. This can be done for any string-crossing angle. The case shown as (c) is for a string-crossing angle of approximately 90 degrees and thus resembles a corner. Situations of near-zero string-crossing angle also occur. In those cases, the viewing angles are nearly the same while the ranges differ. The apparent size of any surface will be greater when seen at the longer distance, and the two sets of data are made consistent by relabelling as empty the flagged cells at the left and right ends.

No pattern has been presented in Fig. 4 for case (d). This pattern is simple, but the corrections are not unambiguous. This pattern occurs when there are reflections. The validity of the reflection interpretation depends upon the relative viewing distances. This case is discussed further in Section 3.

3. MAPS AND ANALYSES

3.1 Laboratory Environment and Robot Navigation

Plotted in Fig. 5 is a portion of the CESAR laboratory which was set up with three objects of different sizes and orientations. There is a 2'x 2' box, a larger 2'x 4' box, and a small 1'x 1' box. All three boxes are tall enough to intercept the sonar viewing plane. Shown in the plot is the location of the back wall of the laboratory. This wall tends to reflect the sonar signals as does the wall on the left-hand side of the room (which is off-scale). Finally, there is a support pillar and an adjacent pair of narrow vertical pipes in the lower right-hand corner of the room. Displayed along with these five "objects" are eight locations along the path taken by the HERMIES-IIB robot. At each of these locations, a 360-degree scan was taken in 24 15-degree steps (except the first position where small angular steps were used).

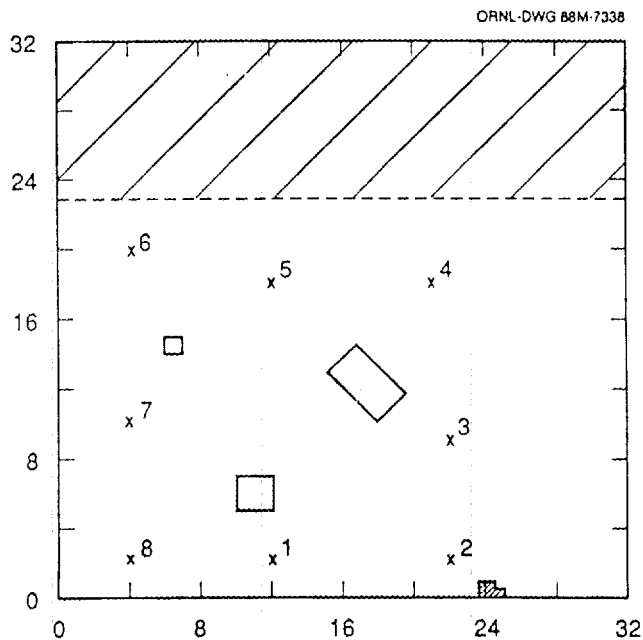


Fig. 5. Schematic diagram of the experimental configuration used in the CESAR laboratory. The numbers show the eight scan locations of the HERMIES-IIB robot; the open squares and the rectangle represent the obstacles. Not shown in the plot is the wall on the left which is located at -1 ft. Also missing is a workstation plus some partitions placed along the right-hand side of the lab in the second of two sets of experiments, and some low-level clutter in the upper right-hand corner during the early experiments.

In navigating about our test environment cumulative dead-reckoning errors can occur. This class of errors has been discussed by Chatila and Laumond[5] and by Drumheller[6]. In their studies a number of solutions were investigated, and those introduced previously in the literature were cited. Spatial uncertainties due to dead-reckoning errors have also been examined by Smith and Cheeseman[23] and by Smith, Self and Cheeseman[24]. In the present work we avoided these errors by explicit placement of the robot at the various test locations. We did this in order to focus our attention on the systematic errors outlined in the introduction. Careful checks done after completion of the experiments showed that cumulative dead-reckoning errors would have been negligible. More generally, a hardware solution to possible dead-reckoning errors, made by mobile robots which must navigate in unstructured terrain, is to use a ring laser gyroscope.

3.2 Instantaneous Scan Maps and Strings

The results of processing the sparse information from a single 360 degree scan are presented in Fig. 6. Any conflicts represented by the patterns shown in Figs. 2 and 4 (a) and (b) have been resolved.

ORNL-DWG 88-7344

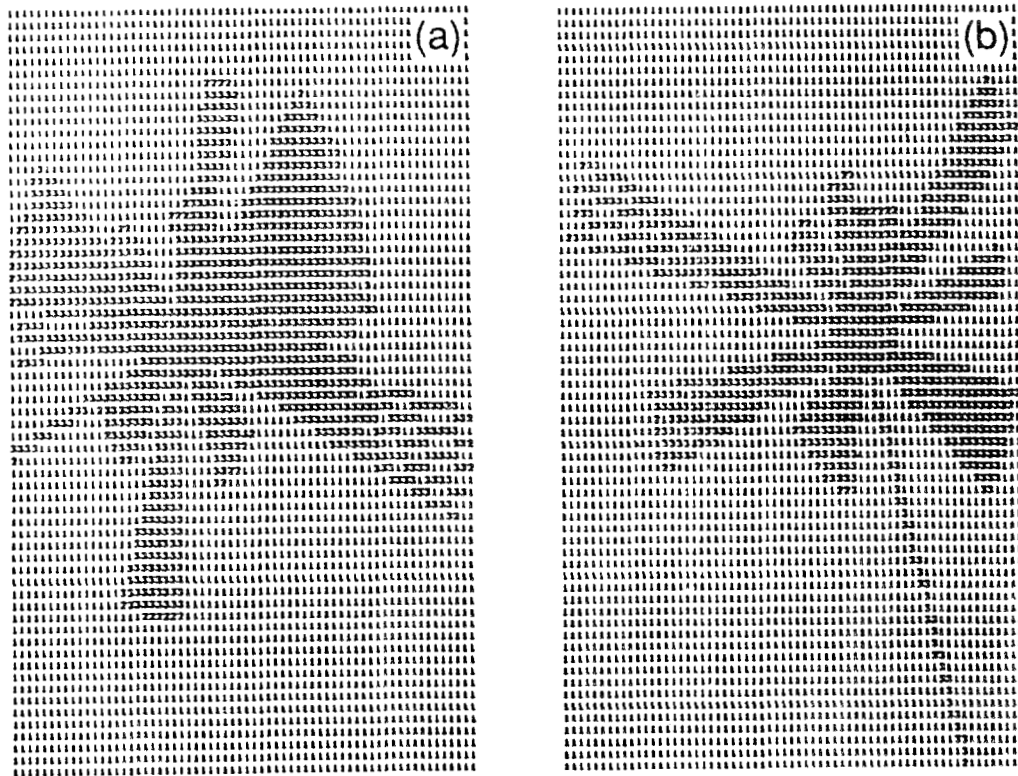


Fig. 6. Instantaneous scan maps. (a): map built from data taken at position 5; (b): map constructed from data acquired at position 4. Maps are 64 x 64 pixels.

At this level of processing conflicts of type (c) have not been identified. Instead, they will be treated during the construction of the cumulative scan map to be described shortly. The dimensions of all maps were chosen as 64 x 64, and each pixel denotes a 6-inch square region of space. The pixels of the instantaneous (single) scan map carry one of three labels, namely, unknown (1), occupied (2) or empty (3).

We observe in Fig. 6 that the measurement serves to partition the space into a number of distinct regions. The most prominent of these are the empty zones fanning out from the robot origin. These zones are terminated by strings, that is, by sequences of neighboring occupied pixels denoting the possible locations of object surfaces. The important strings in, for example, Fig. 6 (a) are located at the ends of the three zones fanning out in a downward direction from the robot origin to the surfaces of the three boxes. To exhibit these strings in a clear visual manner we have suppressed the processing of all but a few long returns for which no echo was received.

The strings represent the extension of the sequences of occupied pixels illustrated in Figs. 2 and 4 to instances where there are more than two contiguous ranges. All discussions regarding the patterns and conflicts are valid for the strings. As such, the strings comprise the first order of feature extraction above the pixel level. Their identification is in this sense comparable to edge detection in the processing of visual images.

It should be observed that in our analysis extended objects are perceived as having smoothly-joined surfaces. There are, for example, no intersecting wedge-shaped objects, and deeply convoluted surfaces will not be seen as such. This aspect is part of our world-view, introduced in Section 2, and is consistent with the physical limitations of the probe (sensor).

3.3 Cumulative Navigation Maps

Displayed in Fig. 7 is a sequence of 8 cumulative navigation maps corresponding to the eight scanning positions shown in Fig. 5. All rays have been included in the scoring. For purposes of visual display, unknown areas have been left blank, occupied regions are marked with 1's and empty zones are shown as 0's. We observe in this progression of maps that regions which are initially occluded or out of range of the sensor are gradually identified, and the outlines of the boxes are built as their various surfaces are illuminated. By the eighth scan all three boxes are delineated.

To construct the cumulative navigation map, we performed a map by map multiplication. That is, the label of ij^{th} pixel in the instantaneous (scan) map was multiplied by the label of the ij^{th} pixel in the previously updated cumulative map, and the results were

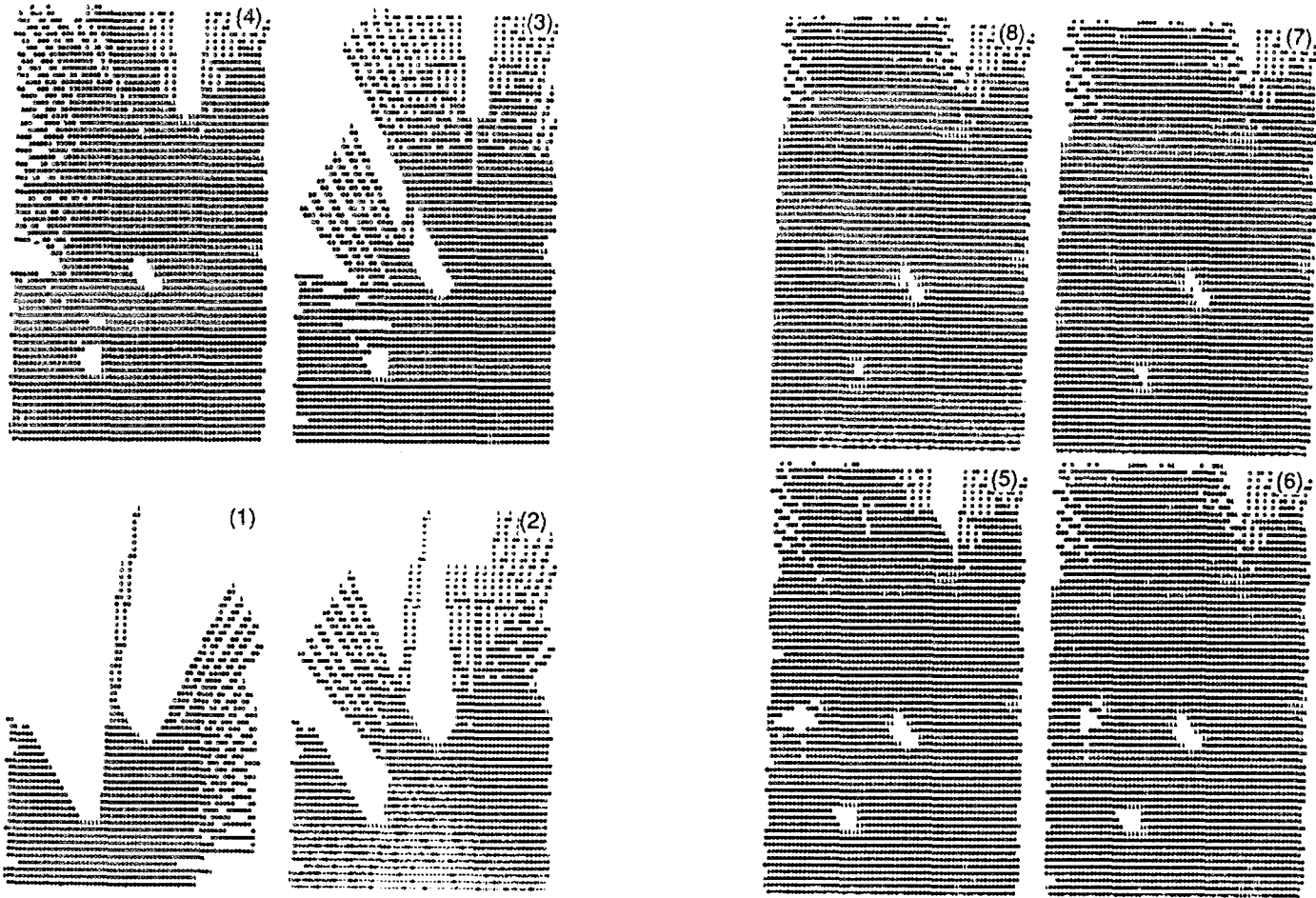


Fig. 7. Cumulative navigation maps. Shown are the navigation maps built following data collection at the eight scan sites displayed in Fig. 5.

stored as the new label of the ij^{th} pixel in the new cumulative map. The label multiplication was done for all pixels using the logic presented in Fig. 3. The pixels of the cumulative map, therefore take on the values conflict (0), unknown (1), occupied (2), or empty (3).

At this point the data were examined for conflict patterns of the type shown as Fig. 2 (c). The pattern analysis was done using auxiliary string maps and ancillary buffers. Stored in the string maps were indices identifying each string. The corresponding x and y coordinates, and the lengths (number of pixel elements), were contained in the buffers. This information was used to rapidly check for string crossings—places where a pair of strings cross through one another. In those instances where this occurred, any conflict labels lying along either of the strings were replaced with empty labels. This snipping operation leads to Fig. 4 (c), and excessive lengths of strings are selectively shortened.

In the next stage of the preparation of the navigation map we make a limited attempt to treat conflict patterns of type (d). Our objective was to minimize the destruction of legitimate occupied labels by the marking of empty pixels during the processing of false echoes (reflections). False echoes most often give rise to long returns, and their incorrect interpretation can give rise to the apparently unphysical pattern shown as (d). If conflicting assignments were encountered between elements of a string seen at short range and empty zones swept out by distant returns, the conflict was resolved by selection of the occupied label. The examination of the pattern was facilitated by the use of a range map into which the original distance or range information for each string was maintained.

3.4 Consistent-Labeling

The final information processing stage consists of converting any residual conflict labels to occupied or empty labels. We carry out this operation by imposing a consistent-labelling requirement, namely, that the selection of the label must be consistent with those of its neighbors. This condition has the effect of cleaning-up (removing) isolated conflict pixel labels. This step is done, as illustrated in Fig. 8, by adding the values of the 4 immediate surrounding pixels. If their sum (threshold value) is 9 or above (i. e., if at least three neighboring pixels are identified as being empty) the conflict label is replaced by an empty label; otherwise the pixel is scored as occupied.

The threshold value is skewed towards retaining occupied labels. The reason for this can be made clear by examining the scoring of the returns from the pillar and pipes located in the lower right-hand corner of the laboratory. The data from the different scan positions were not sufficient for the direct identification of a

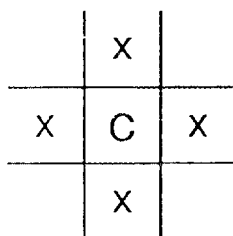


Fig. 8. Diagram of the pixels used for consistent labelling.

well-localized object. Instead, a scattering of conflicting occupied and empty assignments were obtained in the appropriate region of space. The application of the above requirement to this cluster of conflict labels results in the marking of a portion of this region as being occupied, thereby preventing the robot from colliding with these or similar obstacles while navigating.

The optimal threshold value for the consistent label sum depends in part upon the angular stepsize (Section 2.1) used to generate the intermediate rays. The above-mentioned value of 9 is appropriate for a 3 degree stepsize. This angular stepsize, although adequate for short and intermediate distance returns, may miss some of the 6" x 6" pixels at large distances as can be seen in Fig. 6. For such returns, an angular stepsize of 2 degrees will lead to an improved sweep of the cells lying within the beam-cones. As a result of the denser covering generated by the 2-degree stepsize, a lower, less skewed, consistent labelling threshold value of 6 is optimal.

It is still possible for the rays to miss pixels, leaving interior blanks in the maps. This apparent problem can be remedied by an application of a similar consistent labelling algorithm to embedded blank labels. Both types of residual uncertainties (conflict and unknown) are removed by the consistent labelling operations only during the reduction to a binary navigation map. That is, consistent label changes are not retained but instead the algorithms are reapplied each time sensor data are received. This is done to maintain consistency of interpretation among the various data sets.

3.5 Discussion of Results

Poorly-seen objects, such as the support pillars and narrow pipes, are susceptible to elimination from the maps by the scoring of empty spaces from adjacent long returns. Some attention to this type of processing error was given in the resolution of conflict patterns of

Fig. 2 (b) and (d). An example of this sensitivity can be found in Fig. 9, showing a pair of navigation maps. (Two series of experiments were carried out. Map 9 (a) was generated during the first series of experiments; Map 9 (b) was built during the second series. The main difference between the two series of measurements was that Texas Instruments sonar ranging modules SN28827 were used in the first series and Polaroid assemblies 735710 were employed in the second series.) In this figure we tried to highlight the occupied cells. To do this we changed the occupied pixel label to an 'x' and left empty spaces blank. We observe in Fig. 9 (a) that there is no indication of any objects in the lower right-hand corner of the maps, and there is only a slight indication for the objects in Fig. 9 (b). The methodology used in the generation of these maps differed in the treatment of patterns (b) and (d) in what might seem to be a minor way from that finally chosen.

A second observation in Fig. 9 may be made by comparing the two maps to each other. The electronic circuitry of the sensors was improved in the second series of measurements. In Fig. 9 we see that the maps of the second series are not superior to those generated in the first series. In fact, the two larger boxes are more clearly defined in the first map. The reason for this is that the systematic errors increase when the sensitivity is improved.

In Fig. 9 we see that the small, 1' x 1' box appears somewhat larger than its actual size. The systematic size exaggeration has been reduced considerably by the pattern analysis (c) and by the consistent labelling operation. The extent of the reduction can be seen by comparing representation of the box in the instantaneous scan (Fig. 6) maps to that appearing in the cumulative navigation (Figs. 7 and 9) maps. The dependence of the apparent size of objects upon the distance of observation can be observed also, by comparing the lengths of the strings denoting the presence of the box in Figs 6 (a) and (b).

In Fig. 9 (and 8) we see that the back wall of the laboratory does not appear to be well-defined. This wall extends from the left to right side of the room as indicated in Fig. 5. In place of a clearly defined wall we find a few occupied pixels at the correct position plus several strings situated beyond the wall (i.e., in a physically impossible location). These strings, clearly visible in Fig. 6, were produced by our processing of false echoes from the reflecting back wall. In addition to the back wall, the left face of the 2' x 2' box tended to reflect the sonar signals, and as a result, was not as well delineated as the other faces.

Turning to the literature, we note that the strings of pixels lying behind the back wall cannot be removed using the test of Drumheller [6], since we do not assume prior knowledge of the existence of walls, and the back wall is not identifiable. Additional sharpening

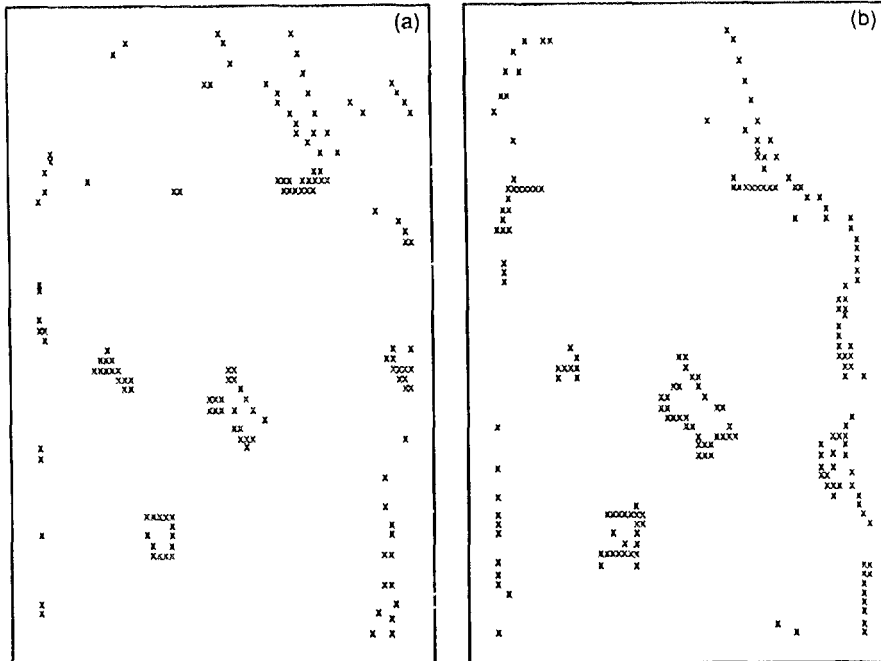


Fig. 9. Cumulative navigation maps at the end of data collection (at scan position 8). (a): first series of experiments; (b): second series.

of object surfaces can be accomplished by performing fits to straight-line segments and to polygons. The usefulness of these object-localization techniques has been demonstrated by Drumheller [6], and by Chatila and Laumond[5], Gaston and Lozano-Perez[12], Grimson and Lozano-Perez[13] and Grimson[14]. In incorporating these techniques one should ensure that the higher-level features so extracted remain consistent with the world-view of the lower-level data processing stage. Finally, we note that effects of errors on the construction of two-dimensional visual maps has been investigated by Brooks[1].

There are a number of possible strategies for reducing uncertainties in object location due to reflections. On a hardware level, we note that bats use a broad range of ultrasonic frequencies for echo location (see, for example, the paper by Fenton and Fullard[9]), and we might try to eliminate sonar reflections by using an adaptive sensor. Sonar reflections from smooth walls have been studied and modelled by Kuc and Siegel[19, 20], and the mathematical problem of finding surface normals has been investigated by Brown[3, 4]. The identification and elimination of false echoes is being addressed further by us in an extension of the present methodology to multisensor fusion. Those results will be reported elsewhere.

4. DISCUSSION OF SOME ALTERNATIVE APPROACHES

Methodologies for the storage of information from sonar range sensors in the form of Cartesian maps have been presented by Elfes [7, 8], Moravec and Elfes[21] and Moravec[22] at Carnegie-Mellon University (CMU), and by Fryxell[11] at ORNL. The CMU methodology makes use of probability distributions, and Fryxell uses a voting procedure to represent initial information on occupied and empty regions of space. In both approaches cumulative information, stored in separate "occupied" and "empty" maps, is used to generate a binary navigation map.

The probability distributions used to interpret the data in the CMU work were functions of the radial distance from the beam origin and the angular distance from the central beam axis. The radial term of the occupied-space distribution was sharply peaked at unity at the distance given by the sensor; the corresponding term in the empty-space distribution was peaked at negative unity at the origin and increased slowly to zero at the point where the occupied-space value went to zero. The angular terms of both distributions were peaked at unity along the central axis and decreased to zero at the edge of the beam cone.

Values $(0,1]$ for the cells (pixels) of the occupied space map were defined as the maximum of the occupied probability distribution over the spatial dimensions of the given pixel. Similarly, values $[-1,0)$ for the cells of the empty space map were set as the minimum of the empty probability distribution. The navigation map was generated by combining the pixel values from the two maps. For a single, isolated return the two distributions are non-overlapping, and their map is identical to ours as given by interpretation (e) of Fig. 1 (except for some smearing of the occupied pixels in the radial direction).

The combination of data from several scans to form an updated navigation map was done in several steps. The empty space map was updated by forming the probabilistic sum of the old and new cell values. The occupied space map was updated by adjusting for non-zero empty space values, renormalizing, and then forming the probabilistic sum. The final step consisted of carrying out a thresholding operation. The thresholding step proved quite useful in "cleaning-up" the navigation map.

In the voting procedure of Fryxell the occupied map pixel located on the beam axis at the distance given by the sensor is incremented by a unit. Then each empty map pixel intercepted by the rays drawn to the robot origin from the occupied coordinate was incremented by a unit. This scoring was done for each scan angle at each robot position. The navigation map was built by first independently normalizing the cumulative occupied and empty sums and then taking

the difference between normalized occupied and empty values for each pixel. If the result was above a certain threshold the navigation map pixel was labelled as occupied; otherwise, it was marked as empty.

In marking empty cells using the voting procedure, a high score will be given to empty pixels near the robot since the rays converge at the origin. Thus, the radial distribution of empty cell scores determined by Fryxell will resemble that obtained by Elfes and Moravec using their probability distribution. The information processing used by Fryxell is that represented in our Fig. 1 (a). Small angular steps of three degrees were taken in order to sweep out the 360-degree region of interest at each scan position. The occupied pixel scoring for a given scan can vary, due to systematic errors, from those of either Elfes and Moravec or the present work.

The probabilistic approaches described above are local in character. That is, the reduction of the various probabilities or votes to one of two labels is done for any given pixel only using information pertaining to that pixel. This type of methodology may be contrasted with our non-local approach, which makes use of information about neighboring cells, as well, and is consistent with the underlying physical processes.

It is, therefore, to be expected that we can build more sharply delineated maps using our method than can be obtained in the alternative, probabilistic approaches. This point was checked in detail by comparing our navigation maps to those constructed by the voting procedure. This was a meaningful comparison, since the same laboratory environment was probed by the identical sensors in both studies. Our finding is that even though five times as much data were collected in the voting experiments, the objects appearing in the maps generated in the present experiments were more clearly delineated. This proved to be the case even when we decreased our cell resolution to match that used by Fryxell.

5. SUMMARY AND CONCLUDING REMARKS

We have presented a methodology for the treatment of systematic errors as they arise in the processing of range information acquired by the HERMIES-IIB mobile robot using its wide angle sonar sensors. Several types of maps, comprising the robot's internal representation of the world, were constructed during the information processing. The navigation maps contained clearly delineated occupied and empty regions; the string and range maps provided information about object surfaces and some sensing conditions.

Four labels were introduced for the purpose of delineating the open, occupied, unknown and conflict cells of the maps. The conflict label denoted those pixels whose identity was uncertain due to conflicts between initial interpretations of the data from different scans. The updating of the navigation maps, i.e., the rule of combination, was done using a simple logic for the four labels. The systematic errors, arising from incorrect interpretations of the data during the processing, manifest themselves as conflict and were flagged by this label as new information was gathered. The essentially binary character of our approach enabled us to do a pattern analysis and impose a simple consistent-labelling condition to remove the conflict. These and the other processing operations we have described are well-established in the field (see, for example, articles by Haralick and Shapiro[15, 16] and Hummel and Zucker [17]), and have been used extensively for different purposes in information processing.

Last, we have taken the first steps to extract progressively higher-level features from the data. This aspect, and the compatibility of our information processing with that of vision, should provide a useful framework for multisensor (sonar + vision) integration.

Acknowledgment

The authors wish to acknowledge the many valuable discussions held throughout the course of this work with R. C. Mann, F. G. Pin and C. R. Weisbin. The authors also wish to acknowledge the assistance provided by D. L. Barnett, E. Lyness and M. Kedl in the HERMIES-IIB experiments. Finally, the authors wish to thank R. Fryxell for making available his ray-scoring routine, which was used with only minor changes in the present work.

References

- [1] R. A. Brooks, "Visual Maps for a Mobile Robot," Proceedings IEEE International Conference on Robotics and Automation, pp. 824-829 (1985).
- [2] B. L. Burks, G. de Saussure, C. R. Weisbin, J. P. Jones, and W. R. Hamel, "Autonomous Navigation, Exploration, and Recognition using the HERMIES-IIB Robot," IEEE Expert, Vol. 2, pp. 18-27 (1987).
- [3] M. K. Brown, "Locating Object Surfaces with an Ultrasonic Range Sensor," Proceedings IEEE International Conference on Robotics and Automation, pp. 110-115 (1985).
- [4] M. K. Brown, "Feature Extraction Techniques for Recognizing Solid Objects with an Ultrasonic Range Sensor," IEEE Journal of Robotics and Automation, Vol. RA-1, pp. 191-205(1985).
- [5] R. Chatila and J.-P. Laumond, "Position Referencing and Consistent World Modelling for Mobile Robots," Proceedings IEEE International Conference on Robotics and Automation, pp. 138-145 (1985).
- [6] M. Drumheller, "Mobile Robot Localization using Sonar," IEEE Transactions Pattern Anal. Machine Intell., Vol. PAMI-9, pp. 325-332 (1987).
- [7] A. Elfes, "Multiple Levels of Representation and Problem Solving using Maps from Sonar Data," Proceedings DOE/CESAR Workshop on Planning and Sensing for Autonomous Navigation, (C. R. Weisbin, Editor), pp. 17-34, Los Angeles, CA. (1985).
- [8] A. Elfes, "A Sonar-Based Mapping and Navigation System," Proceedings IEEE International Conference on Robotics and Automation, pp. 1151-1156 (1986).
- [9] M. B. Fenton and J. H. Fullard, "Moth Hearing and the Feeding Strategies of Bats," American Science, Vol. 69, pp. 266-275 (1981).
- [10] A. Flynn, "Redundant Sensors for Mobile Robot Navigation," M.S. Thesis, Department of Electrical Engineering and Computer Science, MIT, Cambridge, MA. (September, 1985).
- [11] R. C. Fryxell, "Navigation Planning using Quadtrees," ORNL/TM-10481 (CESAR-87/20) (1987).

- [12] P. G. Gaston and T. Lozano-Perez, "Tactile Recognition and Localization using Object Models: The Case of Polyhedra on a Plane," IEEE Transactions Pattern Anal. Machine Intell., Vol. PAMI-6, pp. 257-266 (1984).
- [13] W. E. L. Grimson and T. Lozano-Perez, "Recognition and Localization of Overlapping Parts from Sparse Data in Two and Three Dimensions," Proceedings IEEE International Conference on Robotics and Automation, pp. 61-66 (1985).
- [14] W. E. L. Grimson, "Sensing Strategies for Disambiguating Among Multiple Objects in Known Poses," IEEE Journal of Robotics and Automation, Vol. RA-2, pp. 196-213 (1986).
- [15] R. M. Haralick and L. G. Shapiro, "The Consistent Labelling Problem: Part I," IEEE Transactions Pattern Anal. Machine Intell., Vol. PAMI-1, pp. 173-184 (1979).
- [16] R. M. Haralick and L. G. Shapiro, "The Consistent Labelling Problem: Part II," IEEE Transactions Pattern Anal. Machine Intell., Vol. PAMI-2, pp. 193-203 (1980).
- [17] R. A. Hummel and S. W. Zucker, "On the Foundations of Relaxation Labelling Processes," IEEE Transactions Pattern Anal. Machine Intell., Vol. PAMI-5, pp. 267-287 (1983).
- [18] E. I. Knudsen, S. du Lac and S. D. Esterly, "Computational Maps in the Brain," Ann. Rev. Neurosci., Vol. 10, pp. 41-65 (1987).
- [19] R. Kuc and M. W. Siegal, "Efficient Representation of Reflecting Structures for a Sonar Navigation Model," Proceedings IEEE International Conference Robotics and Automation, pp. 1116-1123 (1987).
- [20] R. Kuc and M. W. Siegal, "Physically Based Simulation Model for Acoustic Sensor Robot Navigation," IEEE Transactions Pattern Anal. Machine Intell., Vol. PAMI-9, pp. 766-778 (1987).
- [21] H. P. Moravec and A. Elfes, "High Resolution Maps from Wide Angle Sonar," Proceedings IEEE International Conference on Robotics and Automation, pp. 116-121 (1985).
- [22] H. P. Moravec, "Certainty Grids for Mobile Robots," Proceedings JPL Workshop on Telerobotics, Pasadena, CA. (January, 1987).
- [23] R. C. Smith and P. Cheeseman, "On the Representation and Estimation of Spatial Uncertainty," International Journal of Robotics Research, Vol. 5, pp. 56-68 (1986).

- [24] R. Smith, M. Self and P. Cheeseman, " A Stochastic Map for Uncertain Spatial Relationships," Proceedings IEEE International Conference on Robotics and Automation, p. 850 (1987).
- [25] W. E. Sullivan and M. Konishi, "Neural Maps of Interaural Phase Difference in the Owl's Brainstem," Proceedings National Academy of Science (USA), Vol. 83, pp. 8400-8404 (1986).
- [26] T. Takahashi and M. Konishi, "Selectivity for Interaural Time Difference in the Owl's Midbrain," Journal of Neuroscience, Vol. 6, pp. 3413-3422 (1986).

DISTRIBUTION LIST

Internal Distribution

- | | | | |
|--------|-------------------|--------|--|
| 1. | B. R. Appleton | 24. | W. W. Manges |
| 2. | S. M. Babcock | 25-29. | R. C. Mann |
| 3. | D. L. Barnett | 30. | S. A. Meacham |
| 4-8. | M. Beckerman | 31. | J. R. Merriman |
| 9. | B. L. Burks | 32-36. | E. M. Oblow |
| 10. | G. De Saussure | 37-41. | F. G. Pin |
| 11. | B. G. Eads | 42. | P. F. Spelt |
| 12. | J. R. Einstein | 43-47. | C. R. Weisbin |
| 13. | C. G. Glover | 48. | B. A. Worley |
| 14. | E. C. Halbert | 49. | EPMD Reports Office |
| 15. | W. R. Hamel | 50. | Central Research Library |
| 16. | J. Han | 51. | ORNL Technical Library
Document Reference Section |
| 17. | J. P. Jones | 52-53. | Laboratory Records |
| 18. | S. M. Killough | 54. | ORNL Patent Office |
| 19-23. | F. C. Maienschein | 55. | Laboratory Records - RC |

External Distribution

56. Office of the Assistant Manager, Energy Research and Development, DOE-ORO, Oak Ridge, TN 37831
57. Dr. J. K. Aggarwal, Computer and Vision Research Center, University of Texas at Austin, Austin, TX 78712
58. Dr. Harry Alter, Advanced Technology Development, Office of Technology Support Programs, U. S. Department of Energy, Washington, DC 20545
59. Dr. Wayne Book, Department of Mechanical Engineering, Georgia Institute of Technology, Atlanta, GA 30332
60. Dr. Rodney Brooks, Artificial Intelligence Laboratory, Massachusetts Institute of Technology, Cambridge, MA 02139
61. Dr. J. S. Coleman, Division of Engineering, Mathematical and Geosciences, Office of Basic Energy Sciences, ER-15, U. S. Department of Energy- Germantown, Washington, DC 20545
62. Dr. J. Dorning, Department of Nuclear Engineering and Engineering Physics, Thornton Hall, University of Virginia, Charlottesville, VA 22901

63. Dr. Alberto Elfes, The Robotics Institute, Carnegie-Mellon University, Schenley Park, Pittsburgh, PA 15213
64. Professor Gene H. Golub, UNIACS -- 2321, Computer Science Building, University of Maryland, College Park, MD 20742
65. Dr. Rafael C. Gonzalez, Department of Electrical and Computer Engineering, University of Tennessee, Knoxville, TN 37996
66. Dr. Robert M. Haralick, Department of Electrical Engineering University of Washington, Seattle, WA 98195
67. Dr. Ewald Heer, Heer Associates, Inc., 5329 Crown Avenue, LaCanada, CA 91011
68. Dr. Avi Kak, Department of Electrical Engineering, Purdue University, Lafayette, IN 47907
69. Dr. Tomas Lozano-Perez, Artificial Intelligence Laboratory, Massachusetts Institute of Technology, Cambridge, MA 02139
70. Dr. Oscar P. Manley, Division of Engineering, Mathematical and Geosciences, Office of Basic Energy Sciences, ER-15, U. S. Department of Energy- Germantown, Washington, DC 20545
71. Dr. H. P. Moravec, Director, Mobile Robot Laboratory, The Robotics Institute, Carnegie-Mellon University, Schenley Park, Pittsburgh, PA 15213
72. Dr. John F. Palmer, Chairman, NCUBE Corporation, 915 E. La Vieve Land, Tempe, AZ 85284
73. Dr. Harry E. Poole, Decision Systems Laboratory, University of Pittsburgh, School of Medicine, Pittsburgh, PA 15261
74. Dr. M. J. Rabins, Dean, College of Mechanical Engineering, Texas A & M University System, 100 Engineering Physics Building, College Station, TX 77843-3123
75. Dr. Karl N. Reid, Dean, College of Engineering, Architecture, and Technology, Oklahoma State University, Stillwater, OK 74074
76. Dr. Melvin W. Siegel, The Robotics Institute, Carnegie-Mellon University, Schenley Park, Pittsburgh, PA 15213

77. Dr. Don Steiner, Department of Nuclear Engineering,
Rensselaer Polytechnic Institute, Troy, NY 12181
78. Dr. Delbert Tesar, Department of Mechanical Engineering,
University of Texas, 26 San Jacinto, Austin, TX 78712.
79. Dr. Mohan N. Trivedi, Department of Electrical and
Computer Engineering, University of Tennessee,
Knoxville, TN 37996
80. Dr. James S. Tulenko, 202 Nuclear Science Center,
University of Florida, Gainesville, FL 32611
81. Dr. David K. Wehe, Department of Nuclear Engineering,
2355 Bonisteel Boulevard, University of Michigan,
Ann Arbor, MI 48109.
- 82-91. Office of Scientific and Technical Information Center,
P. O. Box 62, Oak Ridge, TN 37831.

